Electrochemical characterization of microbial bioanodes formed on a collector/electrode system in a highly saline electrolyte

Raphaël Rousseau, Mickaël Rimboud, Marie-Line Délia, Alain Bergel, Régine Basséguy *

Laboratoire de Génie Chimique, CNRS-Université de Toulouse (INPT), 4 Allée Emile Monso, BP 84234, 31432 Toulouse, France

A B S T R A C T

Bioanodes were formed with electrodes made of carbon felt and equipped with a titanium electrical collector, as commonly used in microbial fuel cells. Electrochemical impedance spectroscopy (EIS) performed on the abiotic electrode system evidenced two time constants, one corresponding to the "collector/carbon felt" contact, the other to the "carbon felt/solution" interface. Such a two time constant system was characteristics of the two-material electrode, independent of biofilm presence. EIS was then performed during the bioanode formation around the constant applied potential of 0.1 V/SCE. The equivalent electrical model was similar to that of the abiotic system. Due to the high salinity of the electrolyte (45 $g \cdot L^{-1}$ NaCl) the electrolyte resistance was always very low. The bioanode development induced kinetic heterogeneities that were taken into account by replacing the pure capacitance of the abiotic system by a constant phase element for the "carbon felt/solution" interface. The current increase from 0 to 20.6 $A \cdot m^{-2}$ was correlated to the considerable decrease of the charge transfer resistance of the "carbon felt/solution" interface from 2.4 10^4 to 92 $\Omega \cdot cm^2$. Finally, EIS implemented at 0.4 V/SCE showed that the limitation observed at high potential values was not related to mass transfer but to a biofilm-linked kinetics.

1. Introduction

Electrochemical impedance spectroscopy (EIS) has been identified by numerous research groups as a powerful tool to investigate electron exchange mechanisms in microbial electrodes [1–2]. The first EIS analyses performed in the domain of microbial electrochemical systems (MESs) have logically been implemented on the pioneering technology of microbial fuel cells (MFCs), generally in order to assess the internal resistance of various cell designs [1,3–7]. As the research domain progressed, studies have started to focus on the detailed characterization of individual microbial electrodes rather than the investigation of whole electrochemical set-ups [1]. EIS has been used to investigate the growth of biofilms on different microbial electrodes [3,8–9], together with the effect of various parameters that influence the charge transfer resistance between biofilm and electrode, such as electrode material [6], pH [5,10], medium ionic strength [11] or the presence of microbially secreted mediators [12]. EIS has also shown the capability to monitor the evolution of the microbial community during the formation of an electroactive biofilm [13].

Most of these studies have been carried out directly in MFC set-ups. It is pretty difficult to extract the basic conclusions on interfacial phenomena in such conditions, because EIS models must take into account the complexity of the whole cell, including the interfacial phenomena on both electrodes [14]. Moreover, in an MFC the potential of each electrode is not controlled but varies as a function of the evolution of the whole cell. The potential of the electrode under study can vary to a great extent in the time required for the electroactive biofilm to be formed, in a way that depends on the configuration of the electrochemical set-up [15]. Surprisingly, EIS experiments performed on microbial electrodes formed in well-controlled electrochemical conditions remain a minority so far [16–19].

Moreover, the microbial anodes implemented in MESs are generally complex multi-material systems. The electroactive biofilms are generally supported by graphite or carbon materials, often with a heterogeneous surface morphology or a porous structure, and electrically connected with wires and/or current collectors made of different materials. Besides, the use of metallic collectors will become unavoidable to overcome the low electronic conductivity of carbon-based materials when scaling up microbial electrodes to large sizes. As a consequence, for analytical purpose and also in the perspective of scaling up, the detailed characterization of the electrode system is of crucial importance for studying microbial electrodes. Characterizing firstly the electrode system in the absence of any biofilm should be an essential prerequisite if sound conclusions are to be extracted from EIS analysis.

In this framework, the objective of the present work was to characterize a microbial anode developed on a hybrid working electrode composed of carbon felt associated with a titanium electrical connector, as often used in MFCs and other MESs. The analysis was performed under controlled potential and EIS was implemented around the

applied potential. Care was taken to identify the impact of the two-material electrode by performing control experiments in the absence of biofilm. The biofilm was then formed using salt marsh sediment as inoculum, which has already proved to be the source of very efficient bioanodes that are able to work in highly saline solutions [20–21]. Actually, the high ionic conductivity of the electrolyte obtained here with 45 $g \cdot L^{-1}$ NaCl represents a great advantage for further scaling-up to large size MESs because it allows minimizing the reactor internal resistance. The objective was here to put together the most possible rigorous experimental conditions to characterize the electrochemical behaviour of these promising bioanodes.

2. Material and method

2.1. Inoculum and media composition

Glass reactors (Schott) with a total volume of 700 mL (200 mL headspace) were filled with 450 mL of nutrient medium inoculated with 50 mL of sediments collected from salt marshes (Gruissan, France). The composition of the nutrient medium was: NH_4Cl 2 $g \cdot L^{-1}$, K_2HPO_4 0.5 $g \cdot L^{-1}$, HCl 37% 46 mL, $MgCl_2 \cdot 6H_2O$ 55 $mg \cdot L^{-1}$, $FeSO_4(NH_4)_2SO_4 \cdot 6H_2O$ 7 $mg \cdot L^{-1}$, $ZnCl_2 \cdot 2H_2O$ 1 $mg \cdot L^{-1}$, $MnCl_2 \cdot 4H_2O$ 1.2 $mg \cdot L^{-1}$, $CuSO_4 \cdot 5H_2O$ 0.4 $mg \cdot L^{-1}$, $CoSO_4 \cdot 7H_2O$ 1.3 $mg \cdot L^{-1}$, BO_3H_3 0.1 $mg \cdot L^{-1}$, $Mo_7O_2(NH_4)_6 \cdot 4H_2O$ 1 $mg \cdot L^{-1}$, $NiCl_2 \cdot 6H_2O$ 0.05 $mg \cdot L^{-1}$, $Na_2SeO_3 \cdot 5H_2O$ 0.01 $mg \cdot L^{-1}$, and $CaCl_2 \cdot 2H_2O$ 60 $mg \cdot L^{-1}$. NaCl 45 $g \cdot L^{-1}$ was also added to get a final ionic conductivity of 10.4 $S \cdot m^{-1}$. Sodium acetate (Sigma-Aldrich) was used as substrate for all experiments. All reactors were placed in a bain-marie with temperature fixed at 40 °C. Before each experiment, oxygen was removed from both liquid and headspace volume by flushing the reactors with nitrogen for 20 min.

2.2. Electrodes and electrochemical protocol

All experiments were performed using a 3-electrode set-up. Counter electrodes were plates of stainless steel 254 SMO (6 × 2 cm, Outokumpu) connected to the electrical circuit with a 1 mm diameter and 10 cm long titanium rod screwed on each. Working electrodes were made of porous carbon felt of 2 cm^2 projected surface area (2 × 1 cm, Mersen) electrically connected with a 1 mm diameter and 10 cm long titanium rod. The working electrode potential was controlled at 0.1 V with respect to a saturated calomel reference electrode (SCE, $Hg/Hg_2Cl_2/KCl_{sat}$, 0.24 V vs. SHE, Radiometer) thanks to a multichannel potentiostat (Biologic, EC-Lab V10.21 software). During chronoamperometries, the average current was recorded every 10 min. A value of 0.1 V/SCE was chosen for anode processing and characterization in accordance with the previous studies of this electromicrobial system [20,21].

Acetate concentration was regularly measured with an enzymatic kit (K-ACETAK, Megazyme). Acetate was regularly added (4 M sodium acetate solution) into the reactors in order to stay in a concentration ranging from 5 to 50 mM to prevent substrate limitation.

Every 6 h, electrochemical impedance spectroscopy (EIS) was automatically performed at 0.1 V/SCE with an amplitude of 10 mV and a frequency ranging from 100 kHz to 100 mHz. Fifty-one frequencies were analysed with 5 points per frequency. The experimental data were fitted using the Zfit tool of the EC-Lab software. A randomization was performed before fitting. The most suitable set of parameter values was determined by minimizing the χ^2 criterion, which expresses the distance between the experimental data and theoretical curve as:

$$\chi^2 = \sum_{i=1}^{n} \frac{\left|Z_{exp}(f_i) - Z_{simul}(f_i, param)\right|^2}{\sigma_i^2} \quad (1)$$

where Z_{exp} (f_i) is the experimental impedance at the f_i frequency, Z_{simul} the impedance given by the theoretical model, *param* the chosen equivalent circuit and σ_i the standard deviation.

Chronoamperometry was performed for 20 days. At the end of the experiments the potential of the working electrode was relaxed and a cyclic voltammetry was performed once a stable open circuit potential (OCP) was reached, starting from OCP to 0.5 V/SCE as the upper limit and back to −0.6 V/SCE at a scan rate of 1 $mV \cdot s^{-1}$.

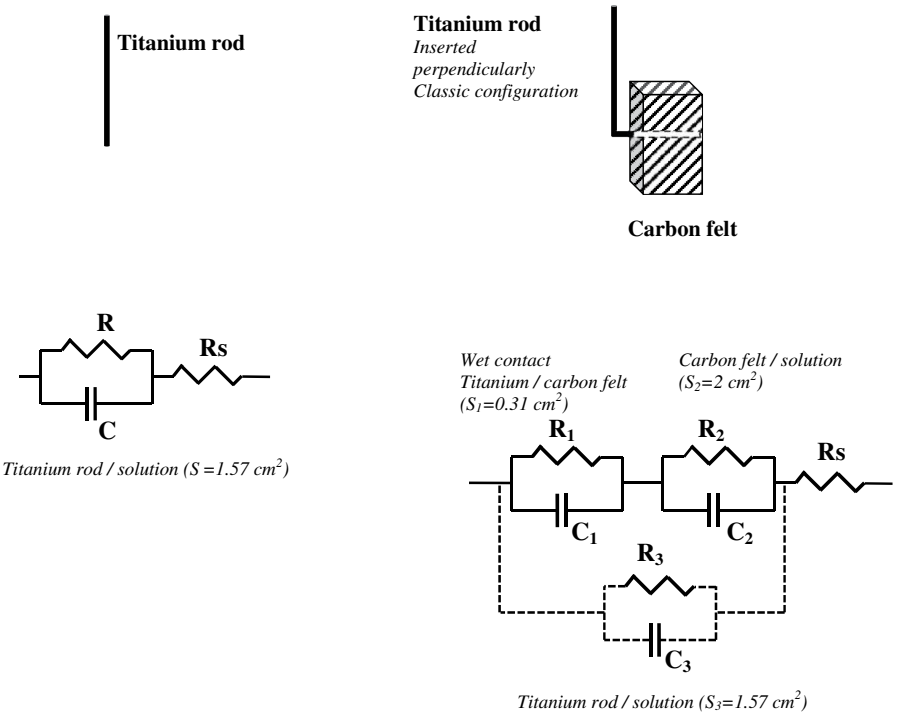

Scheme 1. Scheme of the electrodes and equivalent electrical circuits for the titanium rod and the "titanium rod–carbon felt" electrodes.

For the EIS analysis, the resistance and capacitance of each RC system were reduced to the surface area of the corresponding interface. The titanium rod used alone as electrode, immersed up to 5 cm long, had a surface area exposed to the solution ("titanium rod/solution" interface) of 1.57 cm^2. The "titanium rod–carbon felt" electrode was designed with the titanium rod inserted into the carbon felt perpendicularly to its larger surface area (noted as a classic configuration in Scheme 1), so that 1 cm of rod penetrated the felt. This "titanium/carbon felt" interface had a surface area of 0.31 cm^2. It can be noticed that this contact was always wet due to the high porosity of the carbon felt. The surface areas of the two other interfaces, "carbon felt/solution" and "titanium rod/solution" interfaces, were 2 cm^2 and 1.57 cm^2, respectively (Scheme 1).

3. Results and discussion

3.1. Characterization of the working electrode system without biofilm

Control experiments were carried out without inoculum to characterize the working electrode system in the absence of the electroactive biofilm. During the chronoamperometry at 0.1 V/SCE, only a residual very low current (around 0.2 $mA \cdot m^{-2}$) was detected, which indicated that no oxidation reaction occurred in the absence of the electroactive biofilm. Impedance spectra were recorded during the chronoamperometry (Fig. 1) with the "titanium rod–carbon felt" working electrode and with the titanium rod alone. The titanium rod (Fig. 1A) led to a single phenomenon (arc of circle) with very high impedance. The "titanium rod–carbon felt" electrode gave two clear phenomena (Fig. 1B). At the highest frequencies (from 100 kHz to 6.3 Hz), a semi-circle corresponding to a capacitive loop was observed. The second phenomenon, from 6.3 Hz to 100 mHz, was similar in shape to the one observed with the titanium rod alone, but with a different order of impedance magnitude. In both cases, the spectra remained identical along the 20 days of chronoamperometry.

Firstly, theoretical equivalent electrical circuits were designed on the basis of the physical analysis of the systems (Scheme 1). A usual resistance R_S took into account the ohmic solution resistance in each case. The titanium rod alone implemented a single "titanium/solution" interface, which was modelled by a conventional RC system, i.e. a resistance in parallel with a capacitance. The "titanium rod–carbon felt" electrode displayed three interfaces (Scheme 1): the "titanium/carbon felt" (numbered 1) and "carbon felt/solution" (numbered 2) interfaces, which were in series and, for the part of the titanium rod that was directly exposed to the solution, the "titanium rod/solution" interface (numbered 3), in parallel. Each interface was modelled by a RC system.

Secondly, fitting the experimental Nyquist plots numerically revealed the most suitable equivalent circuits extracted from the experimental data. For the titanium rod alone, the single arc of circle observed in Fig. 1A can be perfectly fitted by a RC system in series with a resistance. For the titanium rod–carbon felt electrode, the fitting circuit was a resistance in series with two RC systems, one corresponding to the semi-circle from 100 kHz to 6.3 Hz, and the second to the arc of circle from 6.3 Hz to 0.1 Hz in Fig. 1B.

The in-series resistance measured for both systems corresponded to the solution resistance (R_S) with values of 1.2 and 1.4 Ω (Table 1). The low electrolyte resistance obtained here was consistent with the high conductivity of the solution (10.4 $S \cdot m^{-1}$), while solutions generally used in the bioelectrochemical systems have much lower conductivities, typically around 2 $S \cdot m^{-1}$ or less [22]. The experimental conditions implemented here were the result of a recent work [20–21] that aimed at designing halotolerant bioanodes. These bioanodes were able to operate in highly saline electrolyte, here the experiments were performed in media containing 45 $g \cdot L^{-1}$ NaCl, which was responsible for the high ionic conductivity.

In the case of the titanium rod electrode, physical analysis and experimental data were totally in accordance: the single arc of circle (Fig. 1A) is well-fitted by one RC system in series with a resistance (Scheme 1). The capacitance value of the "titanium/solution" interface was around 57 $\mu F \cdot cm^{-2}$ (Table 1), perfectly in the range of a double layer capacitance, typically between 10 and 100 $\mu F \cdot cm^{-2}$ [23]. It can consequently be assumed that the resistance calculated for this interface corresponded to a charge transfer resistance. The value of 9.1 10^4 $\Omega \cdot cm^2$ revealed a huge charge transfer resistance, consistently with the poor conductive properties of titanium as anode.

In the case of the "titanium rod–carbon felt" electrode, the equivalent circuit extracted from the experimental data presented only two RC systems, contrary to the physical analysis that suggested three RC systems. In order to assign the RC systems obtained experimentally to those suggested by the physical analysis, a second type of connection was tested by inserting the titanium rod into the carbon felt longitudinally instead of perpendicularly. The Nyquist plot of this second connection type (Fig. 2) was similar to that of the first connection, except for

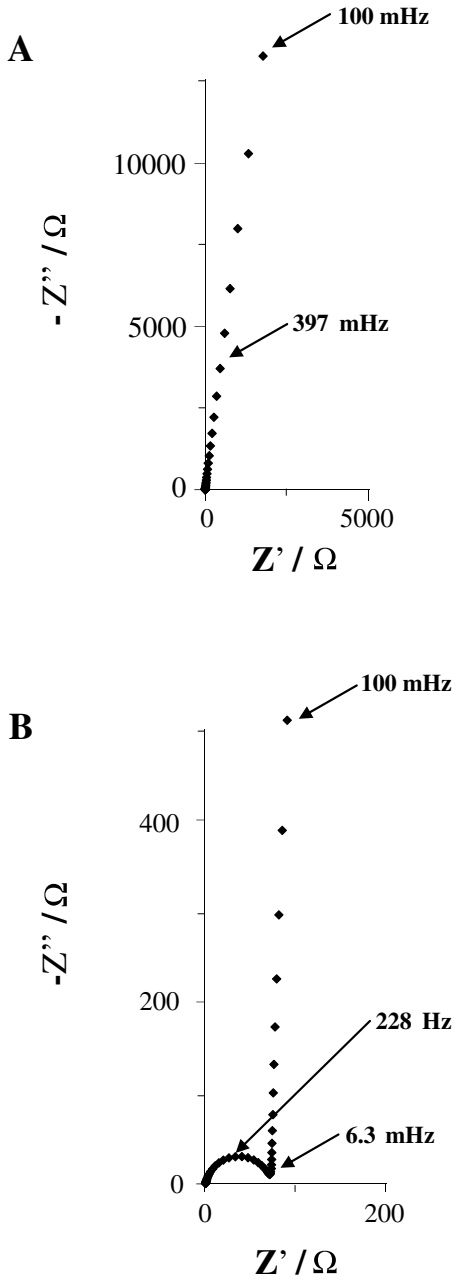

Fig. 1. Impedance (Nyquist plot) recorded during the chronoamperometry at 0.1 V/SCE without inoculum; A. titanium rod alone and B. "titanium rod–carbon felt" electrode. Only the first spectrum (t = 6 h) is presented, the followings obtained during the 20 days of chronoamperometry were identical.

Table 1
Values of the parameters extracted from fitting of the experimental EIS Nyquist plots for each electrode system. Control experiments without inoculation under polarization at 0.1 V/SCE.

Titanium rod electrode					
R_S Ω		R Ω/Ω·cm^{-2}[a]		C F/F·cm^{-2}[a]	χ^2
1.2		$5.8\cdot10^4/9.1\cdot10^4$		$8.9\cdot10^{-5}/5.7\cdot10^{-5}$	1.70
Titanium rod-carbon felt electrode					
R_S Ω	R_1 Ω/Ω·cm^{2}[b]	C_1 F/F·cm^{-2}[b]	R_2 Ω/Ω·cm^{2}[c]	C_2 F/F·cm^{-2}[c]	χ^2
1.4	65.8/20.4	$9.9\cdot10^{-6}/2.9\cdot10^{-5}$	$1.1\cdot10^4/2.2\cdot10^4$	$4.6\cdot10^{-3}/2.3\cdot10^{-3}$	0.97

χ^2 defined by Eq. (1)
[a] Surface area = 1.57 cm^2.
[b] Surface area = 0.31 cm^2.
[c] Surface area = 2 cm^2.

the capacitive loop at high frequencies (19 kHz to 229 Hz), of which the diameter was smaller. Consequently, the RC system at high frequencies (100 kHz to 6.5 Hz) corresponded to the sole characteristics that changed, namely the "titanium/carbon felt" interface (noted R_1C_1 in Scheme 1). The decrease of the diameter of the capacitive loop revealed the anisotropy of the electrode material. Indeed the carbon felt is constituted by carbon fibers that provide a heterogeneous spatial distribution of the material conductivity, which may differ depending on the direction. The "titanium/carbon felt" electrical contact was more effective when the titanium rod passes through the felt in the longitudinal direction (the smallest diameter) than the perpendicular one (the biggest diameter). It was thus confirmed that the RC system at high frequencies corresponded to the "titanium/carbon felt" interface. The resistance and capacitance of the classic perpendicular interface (R_1 and C_1) were respectively 20.4 Ω·cm^2 and 29 μF·cm^{-2} (Table 1). Regarding the resistance value and the type of interface, it cannot be considered here as a double layer behavior, but this interface clearly corresponded to an electrical connection type.

Concerning the phenomenon at low frequencies (6.3 Hz to 100 mHz), a resistance of 2.2 10^4 Ω·cm^2 was found (Table 1). The calculated capacitance was too high (2.3 mF·cm^{-2}) to be considered as a double layer phenomenon. Indeed, the capacitance of a double layer should be between 10 and 100 μF·cm^{-2}. However we basically used the projected surface area of the electrode to calculate the impedance parameters. Regarding the porosity of the material (99%), the carbon felt has a much larger surface area. The calculated value of the capacitance could be consequently diminished by a factor of around a hundred to approach the real capacitance of the electrode material, which would lead to 23 μF·cm^{-2} and would be consistent with double layer behavior. Therefore this RC system can soundly be attributed to the "carbon felt/solution" interface (R_2C_2 in Scheme 1) where R_2 was the charge transfer resistance.

This equivalent circuit extracted from the experimental data presented only two RC systems with a charge transfer resistance R_2 of 1.1 10^4 Ω (S_2 = 2 cm^2) for the "carbon felt/solution" interface and a resistance R_1 of 65.8 Ω (S_1 = 0.31 cm^2) for the "titanium/carbon felt" contact. Both values were significantly lower than the R_3 value of 5.8 10^4 Ω (S_3 = 1.57 cm^2) determined with the titanium rod alone for the "titanium/solution" interface. The experimental circuit with only two RC systems was consequently consistent with the model predicted on the physical analysis of the system circuit that was composed of three RC systems (Scheme 1). The "carbon felt/solution" and "titanium/carbon felt" interfaces in series had a resistance around 5 times lower than that of the parallel "titanium rod/solution" branch (dashed part of the equivalent circuit in Scheme 1). The electrons consequently flowed essentially through the two series RC systems and the third parallel RC system due to the "titanium rod/solution" interface was not detected by EIS.

This kind of equivalent circuit with two serial RC systems has already been used to describe anode systems in microbial fuel cells [12–13]. In these papers, the two RC systems were imputed to the presence of the biofilm. For Ramasamy et al. [12], the occurrence of two time constants was due to the presence of a mediator in the MFC. The first time constant, observed at high frequencies, was attributed to the oxidation of the mediator on the electrode surface, and the second time constant, at low frequencies, was attributed to the reduction of the mediator by the bacterial cells. For Martin et al. [13], the high frequency signal was attributed to the trace of metallic salts and the low frequency signal to the charge transfer between electrode and biofilm.

The present results led to the same kind of RC model without the contribution of any biotic step. This emphasized the great care that must be taken to interpret EIS experimental data coming from microbial electrodes. The detailed analysis of control experiments performed in the absence of biofilm must be a prerequisite, particularly because complex electrode structures are often used to design MFC, including electrical collector and electrode made of different materials. Here the structure of the abiotic electrode was sufficient to produce an equivalent circuit model with two different time constants.

3.2. Characterization of the microbial anodes

3.2.1. Chronoamperometry

Seven reactors were run in parallel: five reactors with a "titanium rod–carbon felt" working electrode and two reactors with only the titanium rod as the working electrode. During chronoamperometry at 0.1 V/SCE (potential in accordance with data from the previous studies that have used this inoculum [20,21]), a current increase was observed for each electrode after a lag time of 4 days for the titanium rod electrodes and 2 days for the "titanium rod–carbon felt" electrodes (Fig. 3). Acetate was added into the reactor in order to maintain a concentration ranging from 5 to 50 mM. In this concentration range, the bioanodes were neither disturbed by acetate depletion nor by acetate inhibition. This regular acetate feeding ensured a continuous current increase until a plateau was reached. At this plateau, current densities were about 3 A·m^{-2} for titanium rods (Fig. 3A) and reached 15.4 to 72.2 A·m^{-2} on "titanium rod–carbon felt" electrodes (Figs. 3B and C).

The variability on the final maximum current densities has already been discussed elsewhere [21]. It was attributed to the heterogeneity of the inoculum composition combined with the large amount used to inoculate (10% *v*/*v*). Nevertheless, the current evolutions observed for the five reactors during the first 10 days were very close, as illustrated in Fig. 3 which reports the two experiments that gave the farthest results. In each case, a current density of around 12 A·m^{-2} was produced on day 10. Actually, the main irreproducibility was lying on the duration of the bioanode development. The reactors mainly differed in the duration of the phase of current increase, likely linked to the phase of biofilm

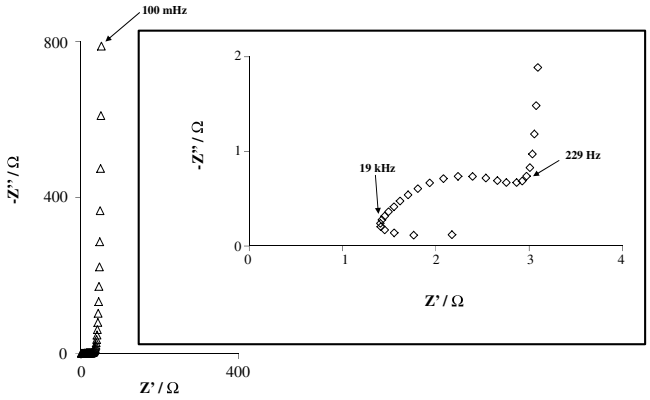

Fig. 2. Impedance (Nyquist plot) of the longitudinal "titanium rod–carbon felt" electrode during chronoamperometry at + 0.1 V/SCE without inoculum.

growth. The first 10-day phase of the bioanode development was reproducible, but the parameter that limited the development of the bioanode and thus defined the value of the maximum current plateau and the time at which it was reached was not mastered.

3.2.2. EIS during bioanode development

Nyquist diagrams were plotted at several times during the 20 days of chronoamperometry (Fig. 4 presents some diagrams obtained during the first 10 days). The first spectra recorded at day 0 just after inoculation were identical to the spectra obtained previously in the absence of inoculum: a single phenomenon for the titanium rod electrode and two phenomena for the "titanium rod–carbon felt" electrode. Then, as the oxidation current increased with time during chronoamperometry, the impedance linked to the phenomenon at low frequencies decreased, corresponding to a lowering of the arc of circle diameter for both titanium rod and "titanium rod–carbon felt" electrodes. The semi-circle at high frequencies, related to the "titanium/carbon felt" contact, did not change throughout the duration of the chronoamperometry.

The evolution of the model parameters during the chronoamperometry are given in Tables 2 and 3 for the titanium rod and the "titanium rod–carbon felt" electrode, respectively. The electrolyte resistance R_S was always very low 1.35 ± 0.5 Ω, in accordance with the values recorded from the control experiments (Table 1). Similarly, the RC system relating to the "titanium/carbon felt" interface was identical to the control and did not significantly

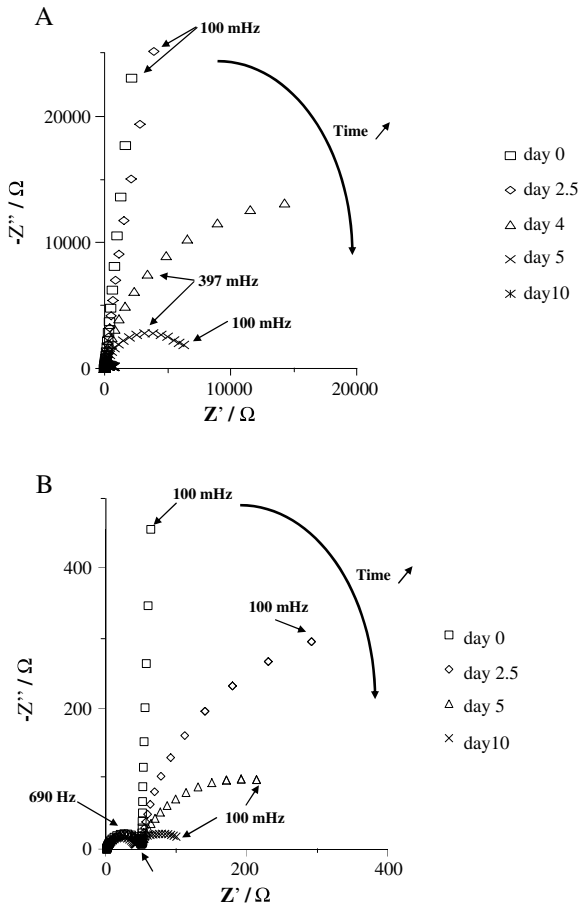

Fig. 4. Evolution of the Nyquist plots with the polarization time; A. titanium rod electrode, B. "titanium rod–carbon felt" system, both inoculated with salt marsh sediment and under polarization at 0.1 V/SCE.

vary throughout the duration of the chronoamperometry (R_1 from 9 to 10 $\Omega \cdot cm^2$; C_1 from 2.4 to 3.3 $\mu F \cdot cm^{-2}$). Due to the thickness of the carbon felt, the micro-organisms did not penetrate deeply inside its structure and did not impact the "titanium/carbon felt" interface.

At low frequency, the capacitive loops were not fully centred on the real impedance axes in the Nyquist plots, contrary to the controls

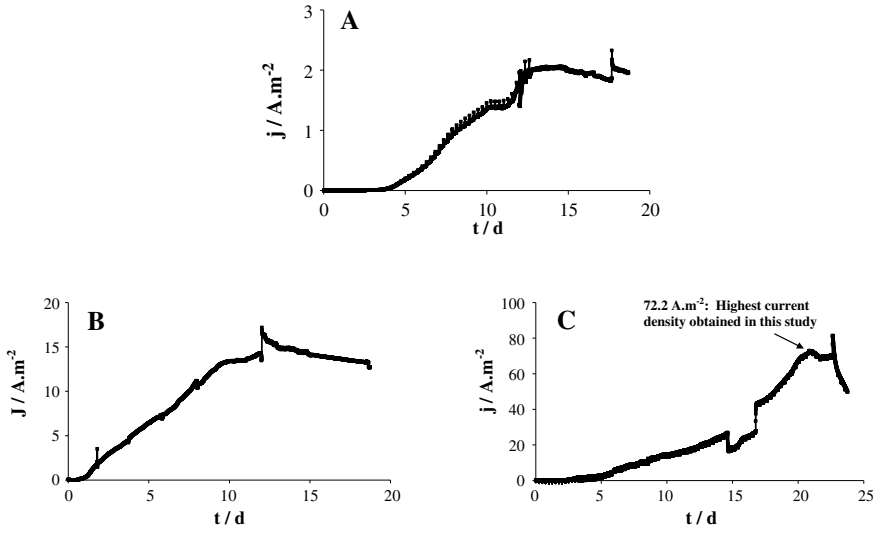

Fig. 3. Evolution of current density with time for a titanium rod electrode (A) and for the "titanium rod–carbon felt" electrodes (B and C) inoculated with salt marsh sediment under polarization at 0.1 V/SCE. Subpanels B and C illustrated the farthest results obtained among 5 replicates.

Table 2
Evolution of current density (j) and impedance parameters during chronoamperometry at 0.1 V/SCE for the titanium rod electrode. Inoculation by salt marsh sediment.

Day	j $A \cdot m^{-2,a}$	R_S Ω	R $\Omega/\Omega \cdot cm^{2,a}$	Q $F \cdot s^{(\alpha-1)}$	α	C_{eff} $F/F \cdot cm^{-2,a}$	χ^2
0	$1.0 \cdot 10^{-3}$	1.6	$7.0.10^4/1.1.10^5$	$5.2.10^{-5}$	0.93	$2.6.10^{-5}/1.6.10^{-5}$	0.02
4	0.04	2.1	$2.1.10^4/3.3.10^4$	$6.7.10^{-5}$	0.81	$8.4.10^{-6}/5.4.10^{-6}$	0.88
8	0.9	1.7	$1.1.10^3/1.3.10^3$	$8.4.10^{-5}$	0.79	$8.0.10^{-6}/5.1.10^{-6}$	0.13
12	1.4	1.6	$4.9.10^2/7.7.10^2$	$5.4.10^{-5}$	0.91	$2.1.10^{-5}/1.4.10^{-5}$	0.20
16	1.9	1.6	$5.9.10^2/9.3.10^2$	$5.1.10^{-5}$	0.90	$1.9.10^{-5}/1.2.10^{-5}$	0.18

χ^2 defined by Eq. (1).
[a] Surface area = 1.57 cm^2.

recorded in the absence of inoculum. This meant that they cannot be considered as pure capacitance. Constant phase elements (CPE) were consequently used to fit the experimental data:

$$Z_{CPE} = 1/Q(\omega)^{\alpha} \times [\cos(\alpha\pi/2) - j\sin(\alpha\pi/2)] \quad (2)$$

where α and Q are the CPE characteristic parameters. In the case of a surface distribution, the equivalent capacity of each interface can be calculated by using Brug's formulae [25]. Brug's formulae depend on the studied system. For the titanium rod, the following equation was used:

$$C_{eff} = Q^{1/\alpha}\left(R_S{}^{-1} + R^{-1}\right)^{(\alpha-1)/\alpha} \quad (3)$$

where C_{eff} is the effective capacitance associated with the CPE. For the "titanium–carbon felt" electrode, a modification must be added to the Brug formulae to take into account the high frequency phenomenon linked to the "titanium/carbon felt" interface (R_1, C_1):

$$C_{eff} = Q_2^{1/\alpha_2}\left((R_S + R_1)^{-1} + R_2^{-1}\right)^{(\alpha_2-1)/\alpha_2}. \quad (4)$$

The values of the α power for each interface were progressively changing with time from 1 to 0.8, according to the shift observed between the real and imaginary parts on the Nyquist plots. In the literature an α value of 0.8 has also been reported for bioanode made on carbon paper [10]. In a general way, values of α smaller than 1 indicate heterogeneities of the current distribution at the electrode surface. These heterogeneities were not provoked by the electrode surface itself because they were never observed in the control experiments performed in the absence of an inoculum or at the beginning of the bioanode formation. The current heterogeneities that progressively increased during the bioanode formation were due to the formation of the biofilm on the electrode surface.

The equivalent capacitances (C_{eff}) calculated for the two electrode systems were of the same order of magnitude than the capacitance measured in the control experiments. Tables 2 and 3 show that the only parameter that changed considerably with time was the charge transfer resistance R for the titanium rod electrode and R_2 for the "titanium rod–carbon felt" electrode. In each case, it corresponded to the interface that was in direct contact with the solution where the biofilm grew. For the titanium rod electrode, the charge transfer resistance R progressively decreased from 110 $k\Omega \cdot cm^2$ to 930 $\Omega \cdot cm^2$, and for the "titanium rod–carbon felt" electrode, R_2 decreased from 24 $k\Omega \cdot cm^2$ to 92 $\Omega \cdot cm^2$. The decrease of the charge transfer resistance was clearly correlated with the development of the electrocatalytic efficiency of the bioanode.

A similar decrease of the charge transfer resistance correlated with an increase of the current or power density provided by an MFC has already been reported in the literature [11]. The charge transfer resistance of a microfibrous carbon paper bioanode has been observed to decrease from 2.6 $k\Omega \cdot cm^2$ to 480 $\Omega \cdot cm^2$ in 3 weeks in an MFC inoculated with a mixed culture from anaerobic sludge and fed with acetate [24]. Martin et al. have observed similar behaviour with the MFC carbon felt bioanode, with a charge transfer resistance of 33 $k\Omega \cdot cm^2$ and 95 $\Omega \cdot cm^2$, obtained 4 and 28 days after inoculation, respectively [13]. In this last study, EIS was implemented at the open circuit potential, where both anodic and cathodic phenomena can occur and must be differentiated to conclude. In the present work, EIS was performed around the applied potential where only oxidation happened. A similar correlation was demonstrated between electrocatalytic efficiency of the bioanode and the considerable decrease of the charge transfer resistance.

3.2.3. Mass transfer or charge transfer limiting

Cyclic voltammetry was performed at the end of a 20-day chronoamperometry for the "titanium rod–carbon felt" bioanodes that had reached their maximum current plateau (Fig. 5A). A significant difference (about 22 A/m^2 i.e. 4.4 mA, Fig. 5A) was observed between the forward and backward scans. This hysteresis phenomenon cannot be attributed to a capacitive current because the scan rate of 1 $mV \cdot s^{-1}$ was too low to produce such a high capacitive current. For example, even considering the highest value of double layer capacitance (C_{eff}) found in our experiments (4.1 mF Table 3), the capacitive current produced at 1 $mV \cdot s^{-1}$ would be 4.1 μA, which would be three orders of magnitude smaller than the currents recorded here. Moreover, a capacitive current would be identical in both scan directions, while a clear dissymmetry was observed here between the forward and backward scans. This hysteresis phenomenon was rather related to the modification of the redox state of some redox components inside the biofilm and should deserve further comprehensive investigation.

Considering only the forward scan, two distinct zones can be differentiated on the j–E curve. In the first zone, between −0.5 and 0.1 V/SCE, the current density increased exponentially with potential. This was a conventional electrochemical activation zone, in which the current is fully controlled by the electrochemical kinetics according to a Butler–Volmer equation for instance. In the second zone, from 0.1 to 0.5 V/SCE, the current did no longer increase exponentially with potential and reached a plateau, here around 35 $A \cdot m^{-2}$, a value similar to the current displayed under chronoamperometry before the voltammetry scan. In the objective to determine the cause of the current limitation observed at high potentials, EIS measurements were performed in both zones: at −0.2 V/SCE for the activation zone and 0.4 V/SCE for the limitation zone. The potential

Table 3
Evolution of current density and impedance parameters during chronoamperometry at 0.1 V/SCE for the "titanium rod–carbon felt" bioanode. Inoculation by salt marsh sediment.

Day	j $A \cdot m^{-2,b}$	R_S Ω	R_1 $\Omega/\Omega \cdot cm^{-2,a}$	C_1 $F/F \cdot cm^{-2,a}$	R_2 $\Omega/\Omega \cdot cm^{2b}$	Q_2 $F \cdot s^{(\alpha-1)}$	α_2	C_{eff} $F/F \cdot cm^{-2,b}$	χ^2
0	0.1	0.9	29/9	$8.6.10^{-5}/2.8.10^{-6}$	$1.2.10^4/2.4.10^4$	$4.1.10^{-3}$	1	$4.1.10^{-3}/2.0.10^{-3}$	0.08
4	5.2	0.9	32/10	$9.3.10^{-5}/3.0.10^{-6}$	$8.3.10^2/1.6.10^3$	$3.1.10^{-3}$	0.97	$2.9.10^{-3}/1.4.10^{-3}$	0.05
8	9.1	0.9	29/9	$8.9.10^{-5}/2.9.10^{-6}$	$1.5.10^2/3.0.10^2$	$3.7.10^{-3}$	0.91	$2.9.10^{-3}/1.5.10^{-3}$	0.06
12	16.8	1.1	33/10	$8.8.10^{-5}/2.8.10^{-6}$	58.3/1.2.10^2	$7.2.10^{-3}$	0.77	$4.1.10^{-3}/2.1.10^{-3}$	0.05
16	20.6	1.0	32/10	$7.5.10^{-5}/2.4.10^{-6}$	46.0/92.0	$5.2.10^{-3}$	0.82	$3.1.10^{-3}/1.6.10^{-3}$	0.05

χ^2 defined by Eq. (1).
[a] Surface area = 0.31 cm^2.
[b] Surface area = 2 cm^2.

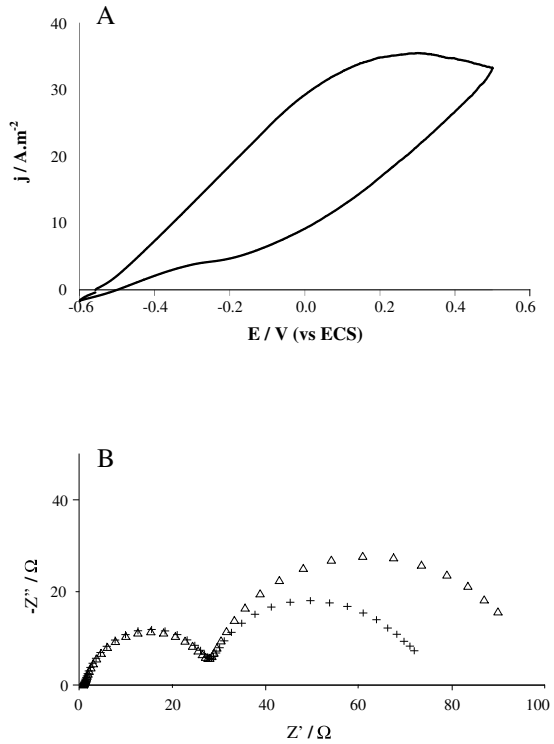

Fig. 5. A. Cyclic voltammogram for the "titanium rod–carbon felt" bionaode at the end of the 20-day chronoamperometry at 0.1 V/SCE; arrows indicate the potential selected for the EIS measurements; B. Nyquist plots of EIS performed at −0.2 V (Δ) and +0.4 V/SCE (+).

was first applied at −0.2 or 0.4 V/SCE for 1 h to get a stable current before EIS was recorded.

Nyquist plots gave the same shape for the two potentials (Fig. 5B) as also previously observed during chronoamperometry: i.e. two consecutive capacitive loops. The diameter of the loop at high frequency was constant whatever the potential (R1 around 30 Ω and C1 around 75–104 μF). The only change was at the low frequency, the diameter of the circle decreased when the potential (and thus the anodic current) was higher and this for various electrodes (Table 4). It can be observed that the term R·I was equal to 0.2 V whatever the potential. Moreover, the values of the capacitance were in the range of 3.1–4.4 mF. Considering the surface of the porous carbon felt (100 × 2 cm^2), the capacitance varied between 16 to 22 μF/cm^2. These two characteristics (constant RI and capacitance in the range of 10–100 μF/cm^2) supported the involvement of a charge transfer phenomenon without any mass transfer contribution. EIS evidenced that a biofilm related kinetics step was rate-limiting rather than mass transfer. Moreover the higher anode potential offered a higher energy for the oxidation reaction and so a greater ease for electrons to pass through the interface, this was consistent with the lower charge transfer resistance obtained at higher potential.

Table 4
Variation of current density and impedance parameters at low frequency for 3 anodic potentials for "titanium rod - carbon felt" bioanodes. Inoculation by salt marsh sediment.

Potential (V/SCE)	Anodic current I (mA)/J (A·m^{-2})	R_2 at LF Ω	$R_2 * I$ V	C_2 F
−0.2[a]	2.7/13.5	66	0.18	$4.4 \cdot 10^{-3}$
0.1[b]	3.4/16.8 (d12)	58	0.20	$4.1 \cdot 10^{-3}$
	4.1/20.6 (d16)	46	0.19	$3.1 \cdot 10^{-3}$
0.4[a]	4.6/23.0	40	0.18	$3.4 \cdot 10^{-3}$

Geometric surface taken into account (2 cm^2).
[a] Experiments of Fig. 5.
[b] Experiments of Fig. 4B.

The present work was innovative by several aspects with respect to the studies that have already implemented EIS to investigate microbial electrodes in MFCs. Firstly, it belonged to the few studies that have been done in potential-controlled conditions using the 3-electrode set-up rather than directly in MFC whole devices. Secondly, EIS was performed here around the applied potential used to form the bioanodes instead of the open circuit potential, as commonly done. EIS has been initiated and developed in the field of corrosion and is generally implemented at the open circuit potential, this means in condition that are most relevant for corrosion research and monitoring. By analogy, several EIS analyses have also been performed on bioanodes at open circuit potential. Here, EIS was performed around the applied potential used to form the bioanodes and then around different applied potentials. This approach enlarges the interest of the method by allowing bioanode characterization in different situations. Here it was shown that the limitation observed at high potentials was not due to mass transfer, as recently observed for *Geobacter sulfurreducens* bioanode for instance [19] but to a biofilm-related kinetics. It should also be noticed that voltammetry significantly disturbed the biofilm electrocatalytic properties, as can be seen by the considerable dissymmetry observed between the forward and backward scans (Fig. 5A). A similar significant perturbation has recently been observed and modelled with microbial oxygen-reducing biocathodes [26]. EIS, which imposes only very small potential perturbations to the electrode may consequently be a powerful method to go ahead in investigating microbial electrodes, particularly when they are sensitive to the applied potential.

4. Conclusion

The characterization of the "electrical collector/carbon felt" system, that was used to support the electroactive biofilms, showed that the abiotic electrode system can generate an equivalent electrical circuit similar to that reported for bioanodes. Two time constants were identified, one corresponding to the "collector/carbon felt" contact and the other to the "carbon felt/solution" interface. Here, the detection of two time constants was consequently not related to the presence of the electroactive biofilm.

EIS was then implemented around the applied potential during the bioanode formation. This led to a simple electrical equivalent circuit, similar to the equivalent circuit of the supporting abiotic electrode. The bioanode development induced kinetic heterogeneities that can satisfactory be taken into account by replacing the pure capacitance by a constant phase element for the "carbon felt/solution" system. During the bioanode formation, the current increase was correlated to the considerable decrease of the charge transfer resistance of the "carbon felt/solution" system. Finally, implementing EIS at different applied potentials showed that the limitation observed at high potential values was not related to mass transfer but to a biofilm-linked kinetics. Work should now be pursued in this direction if the objective is to improve the current densities displayed by these bioanodes.

Acknowledgments

This work was part of the "Défi H12" project financially supported by the "Bioénergies" programme of the French "Agence Nationale de la Recherche" (ANR-09-BioE-010).

References

[1] Z. He, F. Mansfeld, Exploring the use of electrochemical impedance spectroscopy (EIS) in microbial fuel cell studies, Energy Environ. Sci. 2 (2009) 215–219.
[2] X. Dominguez-Benetton, S. Sevda, K. Vanbroekhoven, P. Deepak, The accurate use of impedance analysis for the study of microbial electrochemical systems, Chem. Soc. Rev. 41 (2012) 7228–7246.
[3] A.K. Manohar, O. Bretschger, K.H. Nealson, F. Mansfeld, The polarization behavior of the anode in a microbial fuel cell, Electrochim. Acta 53 (2008) 3508–3513.

[4] Z. He, N. Wagner, S.D. Minteer, L.T. Angenent, An upflow microbial fuel cell with an interior cathode: assessment of the internal resistance by impedance spectroscopy, Environ. Sci. Technol. 40 (2006) 5212–5217.
[5] Z. He, Y.L. Huang, A.K. Manohar, F. Mansfeld, Effect of electrolyte pH on the rate of the anodic and cathodic reactions in an air-cathode microbial fuel cell, Bioelectrochemistry 74 (2008) 78–82.
[6] S. Ouitrakul, M. Sriyudthsak, S. Charojrochkul, T. Kakizono, Impedance analysis of bio-fuel cell electrodes, Biosens. Bioelectron. 23 (2007) 721–727.
[7] A.K. Manohar, F. Mansfeld, The internal resistance of a microbial fuel cell and its dependence on cell design and operating conditions, Electrochim. Acta 54 (2009) 1664–1670.
[8] A.K. Manohar, O. Bretschger, K.H. Nealson, F. Mansfeld, The use of electrochemical impedance spectroscopy (EIS) in the evaluation of the electrochemical properties of a microbial fuel cell, Bioelectrochemistry 72 (2008) 149–154.
[9] A.P. Borole, D. Aaron, C.Y. Hamilton, C. Tsouris, Understanding long-term changes in microbial fuel cells via electrochemical impedance spectroscopy, Environ. Sci. Technol. 44 (2010) 2740–2745.
[10] S. Jung, M.M. Mench, J.M. Regan, Impedance characteristics and polarization behavior of a microbial fuel cell in response to short-term changes in medium pH, Environ. Sci. Technol. 45 (2011) 9069–9074.
[11] D. Aaron, C. Tsouris, C.Y. Hamilton, A.P. Borole, Assessment of the effects of flow rate and ionic strength on the performance of an air-cathode microbial fuel cell using electrochemical impedance spectroscopy, Energies 3 (2010) 592–606.
[12] R.P. Ramasamy, V. Gadhamshetty, L.J. Nadeau, G.R. Johnson, Impedance spectroscopy as a tool for non-intrusive detection of extracellular mediators in microbial fuel cells, Biotechnol. Bioeng. 104 (2009) 882–891.
[13] E. Martin, O. Savadogo, S.R. Guiot, B. Tartakovsky, Electrochemical characterization of anodic biofilm development in a microbial fuel cell, J. Appl. Electrochem. 43 (2013) 533–540.
[14] G. Lepage, G. Perrier, G. Merlin, N. Aryal, X. Dominguez-Benetton, Multifactorial evaluation of the electrochemical response of a microbial fuel cell, RSC Adv. 4 (2014) 23815–23825.
[15] D. Pocaznoi, B. Erable, L. Etcheverry, M.L. Délia, A. Bergel, Towards an engineering-oriented strategy for building microbial anodes for microbial fuel cells, Phys. Chem. Chem. Phys. 14 (2012) 13332–13343.
[16] D. Sridharan, S.P. Manoharan, N. Palaniswamy, Redox behavior of biofilm on glassy carbon electrode, Bioelectrochemistry 82 (2011) 135–139.
[17] A. Ter Heijne, D.P. Strik, H.V.M. Hamelers, C.J.N. Buisman, Cathode potential and mass transfer determine performance of oxygen reducing biocathodes in microbial fuel cells, Environ. Sci. Technol. 44 (2010) 7151–7156.
[18] X. Zhang, M. Epifanio, E. Marsili, Electrochemical characteristics of *Shewanella loihica* on carbon nanotubes-modified graphite surfaces, Electrochim. Acta 102 (2013) 252–258.
[19] J.T. Babauta, H. Beyenal, Mass transfer studies of *Geobacter sulfurreducens* biofilms on rotating disk electrodes, Biotechnol. Bioeng. 111 (2014) 285–294.
[20] R. Rousseau, X. Dominguez-Benetton, M.L. Délia, A. Bergel, Microbial bioanodes with high salinity tolerance for microbial fuel cells and microbial electrolysis cells, Electrochem. Commun. 33 (2013) 1–4.
[21] R. Rousseau, C. Santaella, W. Achouak, J.J. Godon, A. Bonnafous, A. Bergel, M.L. Délia, The electrochemical kinetics of high-salinity tolerant bioanodes is correlated with the structure and microbial composition of the biofilm, ChemElectroChem 1 (2014) 1966–1975.
[22] B.E. Logan, K. Rabaey, Conversion of wastes into bioelectricity and chemicals by using microbial electrochemical technologies, Science 337 (2012) 686–690.
[23] M.E. Orazem, B. Tribollet, Electrochemical Impedance Spectroscopy, John Wiley & Sons Publications, NJ, USA, 2008.
[24] R.P. Ramasamy, Z.Y. Ren, M.M. Mench, J.M. Regan, Impact of initial biofilm growth on the anode impedance of microbial fuel cells, Biotechnol. Bioeng. 101 (2008) 101–108.
[25] G.J. Brug, A.L.G. Van den Eeden, M. Sluyters-Rehbach, J.H. Sluyters, The analysis of electrode impedances complicated by the presence of a constant phase element, J. Electroanal. Chem. 176 (1984) 275—295.
[26] M. Rimboud, E. Desmond-Le Quemener, B. Erable, T. Bouchez, A. Bergel, The current provided by oxygen-reducing microbial cathodes is related to the composition of their bacterial community, Bioelectrochemistry 102 (2015) 42–49.